International Journal of Nanomedicine

Dovepress
open access to scientific and medical research

Open Access Full Text Article

ORIGINAL RESEARCH

Studying the effect of particle size and coating type on the blood kinetics of superparamagnetic iron oxide nanoparticles

This article was published in the following Dove Press journal:
International Journal of Nanomedicine
9 August 2012
Number of times this article has been viewed

Farnoosh Roohi
Jessica Lohrke
Andreas Ide
Gunnar Schütz
Katrin Dassler

MR and CT Contrast Media Research, Bayer Pharma AG, Berlin, Germany

Purpose: Magnetic resonance imaging (MRI), one of the most powerful imaging techniques available, usually requires the use of an on-demand designed contrast agent to fully exploit its potential. The blood kinetics of the contrast agent represent an important factor that needs to be considered depending on the objective of the medical examination. For particulate contrast agents, such as superparamagnetic iron oxide nanoparticles (SPIOs), the key parameters are particle size and characteristics of the coating material. In this study we analyzed the effect of these two properties independently and systematically on the magnetic behavior and blood half-life of SPIOs.

Methods: Eleven different SPIOs were synthesized for this study. In the first set (a), seven carboxydextran (CDX)-coated SPIOs of different sizes (19–86 nm) were obtained by fractionating a broadly size-distributed CDX–SPIO. The second set (b) contained three SPIOs of identical size (50 nm) that were stabilized with different coating materials, polyacrylic acid (PAA), polyethylene glycol, and starch. Furthermore, small PAA–SPIOs (20 nm) were synthesized to gain a global insight into the effects of particle size vs coating characteristics. Saturation magnetization and proton relaxivity were determined to represent the magnetic and imaging properties. The blood half-life was analyzed in rats using MRI, time-domain nuclear magnetic resonance, and inductively coupled plasma optical emission spectrometry.

Results: By changing the particle size without modifying any other parameters, the relaxivity r_2 increased with increasing mean particle diameter. However, the blood half-life was shorter for larger particles. The effect of the coating material on magnetic properties was less pronounced, but it had a strong influence on blood kinetics depending on the ionic character of the coating material.

Conclusion: In this report we systematically demonstrated that both particle size and coating material influence blood kinetics and magnetic properties of SPIO independently. These data provide key information for the selection of a contrast agent for a defined application and are additionally valuable for other nano areas, such as hyperthermia, drug delivery, and nanotoxicology.

Keywords: SPIO, relaxivity, blood half-life, MRI

In recent decades super paramagnetic iron oxide nanoparticles (SPIOs) have attracted increased attention due to their versatility in medical applications, such as drug delivery and hyperthermia, and as contrast agents for magnetic resonance imaging (MRI).[1–3] For all the applications it is essential to know the pharmacokinetic characteristics of the individual SPIOs. Although it is often stated that the pharmacokinetics of SPIOs depends on several parameters, such as size and coating, a systematic examination addressing the influence of the individual parameters is missing. The aim of this

Correspondence: Katrin Dassler
MR CT Contrast Media Research, Bayer Pharma AG, Müllerstr 178, 13342 Berlin, Germany
Tel +49 30 468 12439
Fax +49 30 468 92257
Email katrin.dassler@bayer.com

study was to fill the gap and to prove these statements. The designed setup used herein allows for the precise investigation of the effect of individual parameters on blood kinetics and magnetic properties of SPIOs.

Magnetic properties and blood pharmacokinetics are the key features of SPIOs for MRI. High magnetization is essential for influencing proton relaxivity and thus sensitivity in MRI. The magnetic characteristics are mediated via the magnetite/maghemite iron oxide core. Depending on the synthesis conditions, SPIOs are differentiated in monocrystalline and multicrystalline SPIO.[4] For the latter the core is formed by the clustering of several individual iron oxide crystallites. Due to this clustering the core size is always an average value of a distribution. In this study, we focused on multicrystallite SPIOs.

To prevent the precipitation of iron oxide cores, SPIOs for medical imaging are always coated with a layer of protective colloid, usually a polymer. This polymer acts as a steric and/or electrostatic stabilizer. For biomedical applications it is important that the stabilizer is biocompatible, ie, it must be hydrophilic and nontoxic. The type of surface coating and the polymer chain length on the iron oxide core determine the overall size of the colloid and may also play a significant role in biodistribution, as reviewed by Almeida et al.[5] The surface properties influence uptake by the mononuclear phagocyte system (MPS), also known as the reticuloendothelial system. Finally, uptake could also be affected by the particle core and particle shape.[6,7]

Several studies have indicated that the particle biodistribution is dependent on the sizes and surface properties of the particles.[3,8–10] However, in many cases the conclusion was made using SPIOs, which differ in more than one parameter, making it difficult to differentiate the influence of an individual parameter. We also believe that it is important to compare a set of three or more SPIOs in order to draw a consistent picture.

To analyze the effect of the particle size and coating material on the blood half-life and clearance independently and systematically, we generated two sets of nanoparticulate contrast agents. The first set (a) comprised differently sized SPIOs (19–86 nm) and was obtained by the fractionation of broadly size-distributed carboxydextran (CDX)–SPIOs. In a second set (b), we used different coating materials to stabilize a noncoated SPIO to generate SPIOs of identical size (50 nm) but with different coatings. Herein, if SPIOs are noted to have an identical size, the average size and distribution of the SPIOs are identical. In system b, polyacrylic acid (PAA), starch, and polyethylene glycol (PEG) were used as polymers. The blood pharmacokinetics of these different types of SPIOs (eleven in total) was analyzed in rats, and different methods for the determination of blood half-life and clearance were examined.

Methods

Materials

$FeCl_2 \cdot 4H_2O$, $FeCl_3 \cdot 6H_2O$, nitric acid, potato starch, (3-aminopropyl) triethoxysilane (APS), poly(acrylic acid sodium salt) (PAA, 45% solution in water, molecular weight [MW] 1200 g mol^{-1}), sodium hypochlorite (≥4%), ethylene glycol, and urea were purchased from Sigma-Aldrich (Steinheim, Germany). Sodium hydroxide and glacial acetic acid were purchased from Merck (Darmstadt, Germany). Osmofundin® M-15 (15% mannitol) and Liquemin® solutions were purchased from Braun (Kronberg, Germany). A solution of 1 mol L^{-1} 4-(2-hydroxyethyl)-1-piperazineethanesulfonic acid (HEPES) was purchased from Gibco (Grand Island, NY). N-Hydroxysuccinimide (NHS)-$(PEG)_{12}$-maleimide (PEG, MW 865.92 g mol^{-1}) was purchased from Thermo Fisher (Waldorf, Germany). All chemicals were used without further purification. Water from a Milli-Q water purification system (Millipore, Bedford, MA) was used for all synthesis and dialyzing procedures. P388D1 (IL-1) cells were purchased from American Type Culture Collection (Manassas, VA). Wistar Han rats were obtained from Charles River Laboratories (Sulzfeld, Germany).

Synthesis of SPIOs

Synthesis of noncoated SPIOs

Solutions of 0.8 mmol L^{-1} iron (III) and 0.4 mmol L^{-1} iron (II) chloride were dissolved in 500 mL water and purged with nitrogen for 20 minutes. Under conditions of vigorous stirring and nitrogen purging, 1 mol L^{-1} sodium hydroxide was added drop by drop to the solution until the pH reached 8.6. The system was incubated for additional 45 minutes at room temperature. The black dispersion was washed three times with water and once with 2 mol L^{-1} nitric acid by centrifugation (10 minutes at 769 × g), and the redispersed pellet was sonicated. Finally, the pellet was re-dispersed in 25 mL water. These purified noncoated SPIOs had an average hydrodynamic size of 70 nm and a zeta potential of +40 mV. Due to their charge, the noncoated SPIOs were stabilized via electrostatic shielding.

Synthesis of 50 nm PAA–SPIOs

The concentration of the synthesized SPIOs was set to 30 mmol L^{-1} and a pH of less than 3 using water and 20 µL

nitric acid (2 mol L^{-1}). In total, 12 µL PAA was dissolved in 4988 mL water, and the pH was lowered to below 3 by adding 20 µL of 2 mol L^{-1} nitric acid. In total, 5 mL PAA solution was added to 5 mL SPIO solution. The precipitated SPIO solution was centrifuged for 1 minute. The precipitate was redispersed in water, and the pH was set to 9.0 by adding sodium hydroxide. After 15 minutes in an ultrasound bath, the solution was thoroughly dialyzed against water (molecular weight cut-off [MWCO] 3500 Da, pH set to 7.0). The PAA–SPIOs were concentrated by rotary evaporation. Finally, to remove large particles, PAA–SPIOs were centrifuged at 8000 × g for 8 minutes. The supernatant of the centrifuged raw product was decanted and used for all studies.

Synthesis of 20 nm SPIOs

The reaction was performed under nitrogen in a 4580 Parr pressure reactor equipped with a 5.7-L vessel. The reactor was filled with 2000 mL water, 23.4 g iron(III)chloride hexahydrate and 8.6 g iron(II)chloride·tetrahydrate. The mixture was stirred at 500 rpm and purged with nitrogen for 20 minutes. Subsequently, 34.7 g PAA was dissolved in 150 mL ammonia (25%) at 0°C. This mixture was quickly added to the iron solution at room temperature. The mixture was heated to 150°C, and the crude product was withdrawn after 3 hours. The black dispersion was neutralized to pH = 7.0 by the slow addition of concentrated nitric acid followed by thorough dialysis against water. Excess water was removed by rotary evaporation (in a 70°C water bath) to yield an approximately 15-fold enrichment of iron. Larger particles were removed by centrifugation at 25,000 × g for 30 minutes and the obtained supernatant was used for all studies. The average particle diameter was 20 nm for these PAA–SPIOs.

Synthesis of starch–SPIOs

In total, 0.5 g starch was dissolved in 10 mL boiling water. After complete dissolution, the starch was cooled to 50°C. In total, 8 mL of the starch solution was added to 8 mL of noncoated SPIOs (33 mmol L^{-1} iron) and shaken at 90°C for 170 minutes. After storage at 4°C overnight, the temperature of the solution was increased to room temperature. The solution was mixed with 3.57 mL sodium hypochlorite and incubated at 70°C for 45 minutes. The reaction was quenched by the addition of 1.43 mL urea (8 mol L^{-1}). The final starch-coated SPIOs were thoroughly dialyzed against water (MWCO 100 kDa). The starch–SPIOs were concentrated by rotary evaporation and centrifuged at 8000 × g for 8 minutes. The supernatant was used as a final 50 nm-starch–SPIO batch.

Synthesis of PEG–SPIOs

A total of 480 µL acetic acid was added to 24 mL of SPIOs (110 mmol L^{-1} iron), and the mixture was shaken for 30 minutes at 70°C. Next, 19.2 mL ethylene glycol and 240 µL APS was added to the reaction mixture, which was shaken at 70°C overnight. The APS-coated SPIOs were dialyzed against water at pH = 3.0 overnight (MWCO 3500 Da). Then, 100 mg PEG was dissolved in 20 mL HEPES (15 mmol L^{-1}) and mixed with 20 mL APS–SPIOs (40 mmol L^{-1} iron) for 1 hour at room temperature. The PEG–SPIO dispersion was dialyzed against water (MWCO 3500 Da) and then concentrated by rotary evaporation. SPIOs were centrifuged at 8000 × g for 11 minutes. The supernatant was used as the final 50 nm PEG–SPIO sample. All SPIO solutions were formulated in mannitol using osmofundin to adjust the osmolality. The osmolality was measured in a vapor pressure osmometer 5520 (Wescor/Elitech, Logan, UT).

Preparation of CDX–SPIO fractions with various average diameters

SPIOs were prepared in our laboratory according to the method previously published by Lohrke et al.[11] Briefly, a CDX–SPIO batch was synthesized according to the method described by Hasegawa and Hokkuku.[12] The SPIO suspension was centrifuged 40 minutes at 1500 × g and the supernatant used for the fractionation. Fractionation was performed by magnetic separation using MACS separation XS columns in a CliniMACS cell separation system (both Miltenyi Biotec, Cologne, Germany) at a magnetic field strength of 1 T. After loading the column for 280 seconds with the 500 mmol L^{-1} SPIO solution and a flow rate of 1 mL min^{-1}, elution was started using Aqua ad injectabilia at the same flow rate. Twenty fractions with a volume of 50 mL were collected, ten fractions after starting elution, five fractions after reducing the magnetic field strength to 0.5 T, and another five fractions after switching off the field. The column was washed with Aqua ad injectabilia (Ampuwa, Fresenius, Bad Homburg Germany) for 20 minutes at a flow rate of 2 mL min^{-1}, and the fractionation process was repeated. Finally, fractions were characterized by dynamic light-scattering, and samples with the same hydrodynamic diameter were pooled.

Characterization methods

Transmission electron microscopy

A total of 2 µL of a 0.2 mmol L^{-1} SPIO solution in 50% ethylene glycol or 10% ethanol was dropped onto each transmission electron microscopy (TEM) grid. After incubation for 5 minutes at room temperature, the residual fluid was

removed and the grid was dried for another 5 minutes. The images were taken using an energy-filtered TEM (EM902; Zeiss, Oberkochen, Germany) with acceleration voltage of 80 kV. To determine the crystallite core size, the diameter of $n \geq 50$ cores was measured by ImageJ software (US National Institutes of Health, Bethseda, MA). Results were plotted by frequency analysis using MS Excel (Microsoft, Redmond, WA).

Dynamic light scattering

ZetaSizer Nano-ZS (Malvern Instruments, Worcestershire, UK) was used to determine the hydrodynamic diameters (intensity-weighted Z average) and zeta potentials of the synthesized and fractionated SPIOs at 25°C and pH 7.2 if not indicated otherwise.

Inductively coupled plasma optical emission spectrometry

The iron concentration was determined using an Inductively coupled plasma optical emission spectrometry (ICP–OES) IRIS Advantage ICP (Thermo Fisher Scientific Inc, Waltham, MA). The following parameters were set: sample flow rate 1.5 mL min^{-1}; gas flow rate 0.62 L min^{-1}; plasma gas flow rate 15 L $minute^{-1}$; supporting gas flow rate 0.5 L min^{-1}. For calibration, 2 ppm iron in 5% nitric acid was used. A wavelength of 259.940 nm was selected. To determine the iron concentration, the SPIO samples were dissolved in 30% HCl. After complete dissolution of the nanoparticles (the samples were shaken at room temperature for at least 15 minutes), the solution was dissolved in 100 volumes of 5% nitric acid. For in vivo samples, 100 µL plasma or a 10-µL SPIO solution was mixed with 40 µL yttrium standard (1000 ppm, internal standard), 1.3 mL nitric acid (65%), and 1 mL water and digested using a microwave treatment. The solutions were then diluted with water (4 mL) and analyzed by ICP–OES.

r_1 and r_2 relaxivity

The T_1 and T_2 relaxation times of water protons in the presence of the SPIOs were determined using a 1.41 Tesla (60 MHz) magnetic field in a time-domain NMR (MiniSpec mq 60 Spectrometer, Bruker Optics GmbH, Ettlingen, Germany) at 40°C. The relaxation times for three different SPIO concentrations in water or heparinized plasma were measured. The relaxation rate (1 per relaxation time) was plotted versus the iron concentration. The slope of the linear fit was reported as r_1 and r_2 for each SPIO sample.

Superconducting quantum interference device analysis

Superconducting quantum interference device (SQUID) analysis was performed at the University of Leipzig, Faculty of Physics und Geosciences (Department of Superconductivity and Magnetism), Germany, with a SQUID magnetometer (SQUID MPMS-7, Quantum Design, San Diego, CA), using a reciprocal sample option. The resolution reached 10^{-7} electromagnetic units (emu). The liquid SPIO samples (50 mg of a 50 mmol L^{-1} solution) were embedded in specific drop-shaped vitreous cuvettes with a 5-mm diameter and 15-mm length. Hysteresis curves were monitored at a 300 K fixed temperature and a field strength of –10 to +10 kOe. All measurements were performed in a parallel magnetic field in the longitudinal direction to the cuvette to minimize the background of the diamagnetic part of the cuvette. Based on the signal intensity of the magnetization (emu), the specific magnetization was calculated in emu g^{-1} iron using the exact net weight.

Fourier transform infrared spectroscopy

A Fourier transform infrared spectroscopy (FTIR) spectrometer (Vertex 70, Bruker) was used to acquire infrared (IR) spectra. The SPIO samples were pelleted from dispersion using centrifugation and dried overnight at 60°C. The dried samples were ground with potassium bromide. The mixture (0.3 mg SPIOs and 300 mg KBr) was pressed to obtain a pellet that was then analyzed.

SPIO uptake by P388D1 macrophages

For Prussian blue staining a total of 1×10^5 P388D1 (IL-1) cells were cultured on a chamber slide (Lab Tek II; Nalge Nunc, Naperville, IL) dish for 48 hours. After washing with PBS, cells were incubated for 4 hours with a 1-mL 300-µmol L^{-1} SPIO solution prepared in phosphate-buffered saline (PBS). The solution was replaced by 1 mL ice-cold PBS. Cells were fixed 15 minutes at 4°C in 4% paraformaldehyde. After washing twice with PBS, cells were stained with Prussian blue for 10 minutes (Accustain; Sigma-Aldrich). Excess solution was removed by washing with water. Counterstaining was performed by nuclear fast red (Carl Roth, Kalsruhe, Germany). Slides were embedded in aqueous permanent Ultramount (Dako Cytomation, Hamburg, Germany) and images taken on an Axio Imager Z1 microscope (Carl Zeiss, Göttingen, Germany) with a 63-fold magnification. For quantification a total of 1×10^6 P388D1 (IL-1) cells were cultured in a six-well dish overnight. After washing with PBS, cells were incubated for

4 hours with a 1-mL 300-µmol L^{-1} SPIO solution prepared in PBS. The solution was exchanged by 1 mL ice-cold PBS, and the cells were carefully detached using a cell scraper. After being washed three times in 5 mL PBS, the cells were counted, pelleted by centrifugation, and lysed in 200 µL PBS containing 1% Triton X-100 and 0.6 mol L^{-1} HCL at 60°C overnight. The iron concentration in the lysates was determined using the phenanthroline method according to Saywell and Cunningham or by ICP–OES.[13]

Determination of blood half-life by plasma fractions

To determine the plasma half-life of the SPIO samples, male Wistar Han rats (at least n = 3 per group) were anesthetized by isoflurane (4.0 vol%; Baxter, Unterschleißheim, Germany), nitrous oxide (0.8 L $minute^{-1}$), and oxygen (0.5 L $minute^{-1}$). A catheter was applied to the carotid artery by surgery and directed along the left side of the body to the neck, where the catheter was inserted through the skin. When rats were completely awake (at least 30 minutes after surgery), SPIOs were injected intravenously in the tail vain at a dose of 100 µmol Fe kg^{-1} body weight if not indicated otherwise. For all rats, 0.4 mL blood samples were taken before and 1, 3, 5, 10, 15, 30, 60, 90, 120, and if required 180, 240, and 360 minutes post injection. The lost volume was replaced with a Liquemin®-sodium chloride solution. Finally, the rats were sacrificed. Plasma was isolated, and the iron concentrations in the fractions were determined by relaxation rates in a time-domain NMR (section r_1 and r_2 relaxivity) and by ICP–OES. Plasma taken pre injection served as the blank, and hemolytic samples were excluded. The obtained values were analyzed by WinNonlin software (PharSight Corporation, Mountain View, CA) using a one-compartment model.

Determination of blood half-life by MRI

Wistar Han rats (at least n = 2 per group) were anesthetized by inhalation of 1.5% isoflurane in 1:2 O_2/N_2O and placed in a 3.0 T magnetic resonance tomographic system (MAGNETOM Allegra syngo; Siemens AG, Erlangen, Germany). The SPIO solution was injected via the tail vein at a dose of 100 µmol kg^{-1} after baseline imaging with a wrist coil (CP Wrist OH 44202; USA Instruments Inc, Aurora, OH). Fifty images were acquired for 2 hours and 31 minutes every 2.82 minutes, using a T_2* weighted gradient echo sequence with a repetition time (TR) of 90 milliseconds, an echo time (TE) of 30 milliseconds, a flip angle (FA) of 20°, 8 number of signal averages (NSA) and scan duration 2:49 minutes. The resolution was 640 × 208 pixels at a 2-mm-slice thickness. The signal intensity (SI) changes in the aorta pre and post injection were analyzed. Based on equation (1) for an SPIO signal in a gradient echo sequence, it can be assumed that T_1 is negligible; therefore, the term is reduced to equation (2). Quantity k is a proportionality constant that depends on the sensitivity of the signal detection circuitry on the imager and p is specific to a tissue or pathology. (3) The ln(SI) is proportional to $1/T_2$* and for this reason proportional to the concentration of the contrast agent if the background is subtracted. Hence, concentration changes are expressed as $\ln(SI_{pre}\ SI^{-1}_{post})$ and fitted vs time by first-order kinetics.

1. $SI = k\ p\ (1 - \exp(-TR/T_1))\ \sin\theta\ \exp(-TE/T_2^*)/(1 - \cos\theta\ \exp(-TR/T_1)$
2. $SI = k\ p\ \sin\theta\ \exp(-TE/T_2^*)$
3. $\ln(SI) = -TE\ 1/T_2^*\ \ln(k\ p\ \sin\theta)$

All animal experiments were approved by the governmental review committee on animal care.

Results

Characterization of SPIOs

To systematically examine the influence of particle size and coating material on blood clearance, SPIOs were generated with hydrodynamic diameters ranging from 19 nm to 86 nm. Four different coating materials (PEG, starch, CDX, and PAA) were used. Particles of identical size but different in their coating material were obtained from initially synthesized noncoated SPIOs and a subsequent addition of a layer of PEG, starch, or PAA. Finally, the SPIOs had a medium hydrodynamic diameter of 50 nm and a crystallite size of 11 nm within the particle cluster (Table 1). Representative TEM images of the PEG–, starch–, and PAA–SPIO50 are shown in Figure 1A, including crystallite size-distribution plots. PAA–SPIOs and CDX–SPIOs were generated with different hydrodynamic diameters: PAA–SPIO diameters were 20 and 50 nm and CDX–SPIO diameters were 19–86 nm (Table 1). The low polydispersity index values (<0.2) indicated a narrow size distribution of the particles. All SPIO fractions (CDX particles), regardless of their hydrodynamic particle sizes, showed the same crystallite size within the particle cluster (Table 1 and Figure 1). Successful coating of the SPIOs was demonstrated by FTIR analysis (Figure 1B). All SPIOs showed a characteristic FeO peak at 570 cm^{-1}. The sharp absorption peak at 1380 cm^{-1} for the noncoated SPIOs was due to the presence of nitrate ions on the surfaces of the SPIOs. Nitrate ions were present during the washing process of the noncoated SPIOs. The appearance of the absorption band between 1690 and 1750 cm^{-1} corresponded

Table 1 Physicochemical characterization of different SPIOs

SPIO sample	d_H[a] [nm]	PDI[b]	d_{core}[c] [nm]	ξ-potential[d] [mV]	Ms[e] [emu g^{-1}]	r_1[f] in water [L $mmol^{-1}$ s^{-1}]	r_2[f] in water [L $mmol^{-1}$ s^{-1}]	r_1[f] in plasma [L $mmol^{-1}$ s^{-1}]	r_2[f] in plasma [L $mmol^{-1}$ s^{-1}]
CDX–SPIO20	19	0.191	4.5 ± 0.9	−20	75.7 ± 1.5	13.19 ± 0.05	49.4 ± 0.2	10.8 ± 0.1	51 ± 2
CDX–SPIO35	36	0.135	3.8 ± 1.4	−38	76.3 ± 8.2	12.1 ± 0.1	141.5 ± 0.2	9.1 ± 0.1	158 ± 3
CDX–SPIO50	51	0.149	4.1 ± 0.9	−30	84.0 ± 3.8	9.7 ± 0.1	239 ± 1	6.8 ± 0.1	266 ± 9
CDX–SPIO60	61	0.139	4.6 ± 1.4	−30	94.0 ± 4.5	8.8 ± 0.1	303 ± 1	6.5 ± 0.1	314 ± 3
CDX–SPIO65	64	0.136	nd	−34	92.8 ± 8.5	8.80 ± 0.09	320 ± 2	6.6 ± 0.2	339 ± 9
CDX–SPIO70	72	0.125	nd	−27	95.1 ± 5.3	8.24 ± 0.07	318 ± 1	6.0 ± 0.2	325 ± 1
CDX–SPIO85	86	0.137	5.4 ± 1.0	−32	74.9 ± 1.8	7.3 ± 0.04	339 ± 4	6.3 ± 1	276 ± 11
PEG–SPIO50	52	0.13	11.1 ± 3.6	−20	nd	11.9 ± 0.8	262 ± 24	13 ± 2	283 ± 1
Starch–SPIO50	51	0.13	10.7 ± 3.5	−25	nd	11.3 ± 0.4	241 ± 1	10.5 ± 0.7	269 ± 19
PAA–SPIO50	49	0.13	11.0 ± 3.1	−40	nd	18.0 ± 0.3	287 ± 10	14 ± 5	309 ± 16
PAA–SPIO20	17	0.17	10.9 ± 3.2	−13	nd	16.4 ± 1.6	54 ± 4	16 ± 1	73 ± 6

Notes: [a]Intensity-weighted hydrodynamic diameter d_H (z average) obtained by dynamic light scattering in triplicate with n = 5; [b]polydispersity index (cumulants method); [c]iron oxide crystallite core diameter d_{core} determined by TEM, size of n ≥ 50 cores was measured and given as a mean value and standard deviation; [d]mean zeta potential obtained in water at pH 6 with n = 6 of 30 runs; [e]saturation magnetization calculated from SQIUD data by a bifunctional Langevin fit; [f]relaxivity obtained at 40°C and 1.41 T with standard deviation.

Abbreviations: emu, electromagnetic unit; H, magnetic field strength; M, magnetization; nd, not determined; PDI, poly dispersity index; r, relaxivity; SQUID, superconducting quantum interference device.

to the carbonyl groups (νC = O) in PAA, oxidized starch, CDX, and modified PEG. The presence of carbonyl groups in starch-coated SPIOs was due to the conducted mild oxidation of starch during SPIO synthesis, resulting in the oxidation of hydroxyl groups. (C–O–C) groups in PEG and starch could be characterized via their absorption peak at 1100 cm^{-1} (νC–O–C). The absorption peak between 1200 and 1300 cm^{-1} was related to C–OH vibrations (νC–OH) in PAA, CDX, and starch. FTIR spectra confirmed the successful polymer coating of the SPIO surfaces.

A key parameter for MRI performance with SPIOs is the influence on the proton relaxivity. Relaxivity was measured in water and plasma (Table 1), and was correlated with hydrodynamic size, as shown in Figure 2B. The SPIOs r_2 relaxivity increased with a hydrodynamic size up to 60 nm and remained constant for larger particles. For the 50-nm SPIOs, no considerable differences in r_2 were observed with different types of coatings (Figure 2B). Compared to r_2 relaxivity, r_1 relaxivity showed an inverse but less pronounced effect without exhibiting a threshold value (Figure 2A). The

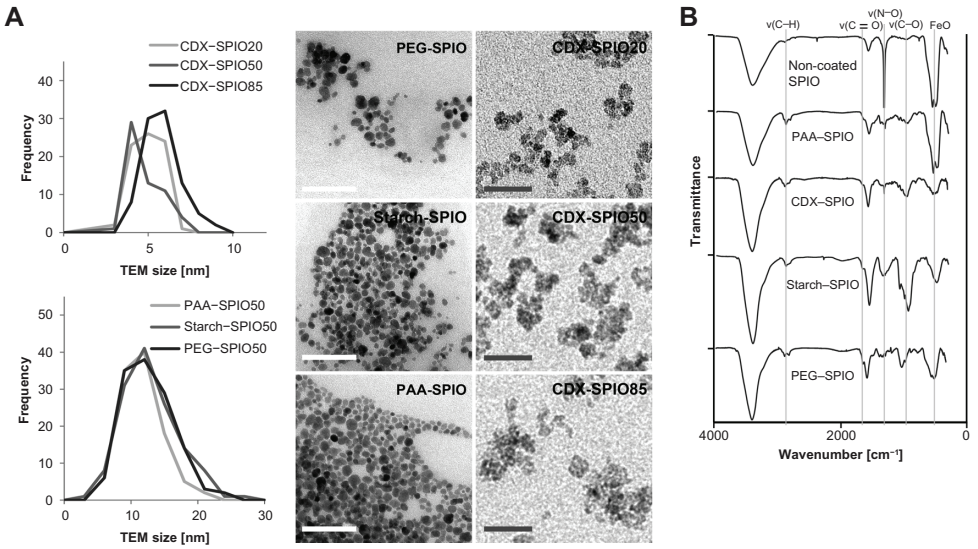

Figure 1 SPIO core diameters were determined by transmission electron microscopy. (**A**) Representative TEM images of CDX–SPIO20, CDX–SPIO50, CDX–SPIO85, PEG–SPIO50, starch–SPIO50, PAA–SPIO50. White bars represent 100-nm scale, gray bars 30-nm scale. Crystallite core diameter distributions for the different sized CDX–SPIOs are shown in the upper plot and distributions for the differently coated SPIOs in the lower plot. Distribution was determined by measuring n ≥ 50 cores per SPIO type. Mean core diameter and standard deviation of all SPIO types are also presented in Lohrke et al.[11] FTIR spectra of all 50 nm SPIOs are shown in (**B**).

Abbreviations: CDX, carboxydextran; FTIR, fourier transform infrared spectroscopy; PAA, polyacrylic acid; PEG, polyethylene glycol; SPIO, superparamagnetic iron oxide nanoparticle.

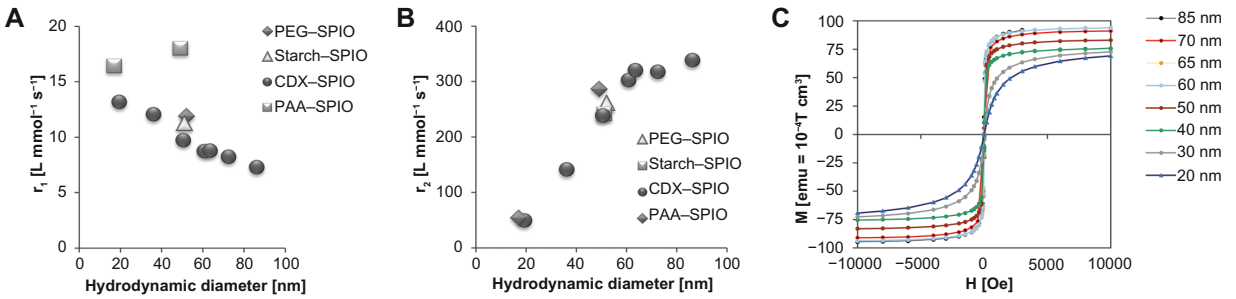

Figure 2 Size and coating dependency of proton relaxivity and magnetic characteristics. Longitudinal (**A**) and transversal (**B**) relaxivity are shown to be dependent on particle size. Relaxivities were determined at 40°C and 1.41 T. M/H hysteresis curves (**C**) represent the change of magnetization (emu g^{-1} iron) at increasing field strengths for the different CDX fractions at 300 K in aqueous solution as measured by SQUID.

Abbreviations: CDX, carboxydextran; emu, electromagnetic unit; H, magnetic field strength; M, magnetization; PAA, polyacrylic acid; PEG, polyethylene glycol; SPIO, superparamagnetic iron oxide nanoparticle; SQUID, superconducting quantum interference device; r, relaxivity.

effect of size on r_2 relaxivity is explained by the enhanced magnetic perturbations caused by the particle core. To measure the magnetic behavior of the differently sized particles in physiologically relevant conditions, a SQUID was used to analyze the SPIOs in solution at 300 K. Representative M(H) curves for CDX–SPIOs with hydrodynamic diameters between 19 and 86 nm are shown in Figure 2C. The saturation magnetization ranged from 75 to 95 emu g^{-1} iron (Table 1). For all SPIOs, the saturation magnetization was achieved at a field strength of less than 1.5 T, which is a clinically relevant field strength. When the magnetic field was reduced to zero, all magnetization curves fell back to zero.

Dose dependency of blood kinetics

Knowledge of the blood half-life and clearance is essential for all medical applications. First, the dose dependency on blood half-life was analyzed with CDX–SPIO20 by the determination of the iron concentration in plasma fractions that were taken at time points between 0 and 360 minutes (Figure 3). An increase in the plasma half-life was observed with increasing doses, ranging from 12.5 to 100 µmol kg^{-1}. However, plasma iron concentrations below 0.01 mmol L^{-1}, as observed at low doses for later time points, were at the detection threshold of this method. Therefore, all further animal experiments were performed with an injection dose of 100 µmol kg^{-1}.

Influence of detection method on the determination of blood half-life

In addition to determining the plasma iron concentration by ICP–OES, the blood half-life can be determined by signal intensity changes in T_2*-weighted MR measurements of blood vessels as well as by determining the relaxation rate in plasma samples using a time-domain NMR. To estimate the robustness of the different techniques, we determined the blood half-lives of five SPIO samples, using distinct detection methods. Representative plots are shown in Figure 4. The signal intensity (SI) of the aorta in T_2*-weighted MR images was analyzed pre-iv and post-iv injection of the CDX–SPIO20 sample (Figure 4A). The corresponding $\ln(SI_{pre}\ SI^{-1}_{post})$ can be assumed to be proportional to the SPIO concentration because T_1 is negligible. In Figure 4B, the kinetics of $\ln(SI_{pre}\ SI^{-1}_{post})$ were demonstrated in comparison to the kinetics of the plasma relaxation rate change (Figure 4C) and plasma iron concentration (Figure 4D). The blood half-life was calculated by fitting a first-order rate

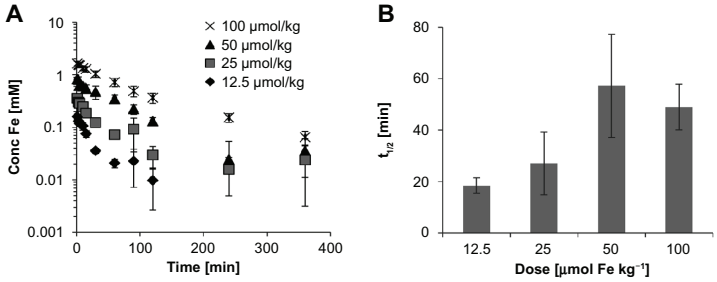

Figure 3 Dose dependency of blood kinetics. CDX–SPIO20 was injected into rats ($n \geq 3$ per group) at doses of 12.5, 25, 50, and 100 µmol kg^{-1}. Plasma samples were taken at indicated time points to determine the plasma iron concentration (**A**). Mean half-lives are summarized in (**B**).

Note: Error bars represent standard deviations of the mean.

Abbreviations: CDX, carboxydextran; SPIO, superparamagnetic iron oxide nanoparticle.

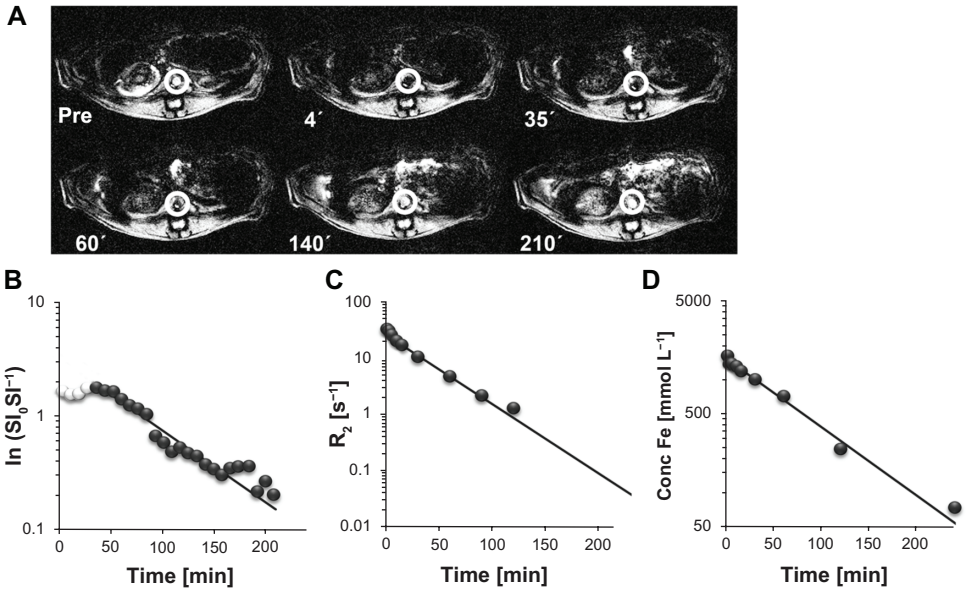

Figure 4 Comparison of different methods to determine the CDX–SPIO20 blood half-life. (**A**) T_2*-weighted transversal MR images were acquired pre and post injection of CDX–SPIO20 application iv in rats and are shown here at representative time points. (**B**) Signal intensities pre (SI_0) and post injection (SI) of the aorta (white circles in A) were analyzed to obtain blood clearance. The first values (white spheres) with constant low signal intensities were not used for the fit. (**C**) R_2 relaxation rates of plasma samples taken from 3 minutes to 360 minutes were determined at 40°C and 1.41 T in a time-domain NMR. (**D**) The iron concentrations in the same plasma samples were measured by ICP–OES.

Note: The values were plotted versus time and fitted by single-order kinetics.

Abbreviations: CDX, carboxydextran; ICP-OES, inductively coupled plasma optical emission spectroscopy; iv, intravenous; MR, magnetic resonance; R, relaxation rate; SI, signal intensity; SPIO, superparamagnetic iron oxide nanoparticle.

equation, assuming a one-compartment model. The results for the different SPIO samples are summarized in Table 2. Comparable values for plasma half-life were calculated with all three methods, although each method has limitations. The standard deviation was highest for the MRI method. Moreover, in MRI early time points were excluded from the fit because directly after injection, the SPIO concentration is high, and the signal intensity is nearly zero; the concentration decreased over time, but the signal intensity stayed low up to a certain concentration.

The plasma relaxation rate has the advantage that the signal is generated directly by the SPIOs. The iron content of the metabolized SPIOs was not detected. However, although MRI and relaxation rate determinations are highly specific for particulate iron oxides, they are indirect methods, assuming that the SPIOs remain nearly unchanged during the time frame of the investigation. In contrast, ICP–OES is superior for the assessment of the overall iron content, as all matrix effects can be neglected when using the appropriate calibration. However, the natural abundance of iron in biological (in this case, plasma) samples must be considered, and if feasible a background correction must be conducted. The least-biased method is the determination of iron in plasma samples by ICP–OES. We have shown that different quantification methods yield similar reliable results. For all further SPIO samples, the iron determination was made by the ICP–OES method, analyzing blood kinetics via iron determination in plasma.

Table 2 Comparison of selected SPIO blood half-lives in rats determined by different methods

Method	Fe conc in plasma	r_2 in plasma	MR signal in aorta
SPIO sample	**$t_{1/2}$ [minutes]**		
CDX–SPIO20	49 ± 10	25 ± 3	38 ± 10
CDX–SPIO50	5.0 ± 0.5	nd	9 ± 1
CDX–SPIO70	2.9 ± 0.4	2.8 ± 0.4	5 ± 2
PAA–SPIO50	4.5 ± 0.4	3.8 ± 0.2	nd
PAA–SPIO20	25 ± 1	21 ± 3	nd

Note: Errors are given as standard deviations of the mean.

Abbreviations: CDX, carboxydextran; MR, magnetic resonance; PAA, polyacrylic acid; r, relaxivity; SPIO, superparamagnetic iron oxide nanoparticle.

Dependency of blood half-life on coating and size

The blood kinetics of all SPIO types were analyzed with a dose of 100 μmol kg^{-1}. The half-life, clearance, and distribution volume were calculated on the basis of the iron concentration in the plasma samples (Table 3). The correlation of half-life with SPIO size and coating is shown in Figure 5. At a constant iron dose, the blood half-life is clearly size dependent. Larger SPIOs have shorter blood half-lives for both PAA–SPIOs and CDX–SPIOs. For 60 nm

Table 3 Plasma kinetics in rats for all SPIO types

Parameter / SPIO sample	$t_{1/2}$ [minutes]	c_{max} [mmol L^{-1}]	Clearance [mL $minute^{-1}$ kg^{-1}]	V_{ss} [L kg^{-1}]
CDX–SPIO20	49 ± 9	1.4 ± 0.4	1.1 ± 0.5	0.074 ± 0.02
CDX–SPIO35	16 ± 3	1.0 ± 0.02	4.3 ± 0.6	0.096 ± 0.002
CDX–SPIO50	5.0 ± 0.5	0.98 ± 0.06	14.4 ± 0.6	0.103 ± 0.006
CDX–SPIO60	4.0 ± 0.8	1.0 ± 0.1	18 ± 6	0.097 ± 0.012
CDX–SPIO70	2.9 ± 0.4	0.54 ± 0.11	47 ± 16	0.19 ± 0.04
CDX–SPIO85	2.8 ± 0.9	1.0 ± 0.2	27 ± 8	0.10 ± 0.02
PEG–SPIO50	28 ± 3	2.7 ± 0.5	1.0 ± 0.2	0.041 ± 0.008
Starch–SPIO50	12.8 ± 1.4	2.6 ± 0.2	2.7 ± 0.4	0.049 ± 0.004
PAA–SPIO50	4.5 ± 0.4	2.25 ± 0.06	8.3 ± 0.8	0.054 ± 0.001
PAA–SPIO20	25 ± 1	3.1 ± 0.9	1.1 ± 0.4	0.04 ± 0.01

Notes: Plasma samples were collected at time points of 1 to 360 minutes post injection of 100 μmol Fe kg^{-1} in rats. Values were calculated based on the iron concentrations in the plasma samples. Errors are given as standard deviations of the mean ($n \geq 3$).
Abbreviations: CDX, carboxydextran; PAA, polyacrylic acid; PEG, polyethylene glycol; SPIO, superparamagnetic iron oxide nanoparticle.

and larger sizes, the average hydrodynamic diameters do not result in a significant decrease in half-life ($P > 0.1$ in a *t* test). Among the different 50-nm SPIOs, PAA–SPIOs displayed the shortest blood half-life, followed by CDX–SPIOs, starch–SPIOs, and PEG–SPIOs. The dependency was attributed to the different ionic characteristics of the coatings.

Influence of coating and size on uptake by macrophages

SPIOs are blood-pool contrast agents, and their pharmacokinetics are mainly dependent on clearance by the MPS. To analyze the uptake of different SPIOs by macrophages, a reproducible in vitro system for phagocytosis/pinocytosis was selected. Cells of the macrophage cell line P-388D1 were incubated with the different SPIOs at a physiologically relevant concentration of 300 μmol L^{-1}. The assay was performed in PBS to control SPIO size in the incubation time by dynamic light scattering. The uptake into cells was analyzed via Prussian blue stain (Figure 6A). Phagocytized SPIOs were mainly located proximal to the nucleus, indicating an irreversible trafficking to the endolysosomal compartment. SPIOs were taken up by an active temperature-dependent process. No Prussian blue staining was observed at 4°C. SPIO uptake was quantified by determination of cellular iron levels (Figure 6B). Larger CDX–SPIOs (up to 60 nm) were correlated with higher iron uptake. For even larger SPIO diameters, iron uptake was not further enhanced. Uptake by macrophages was also influenced by the coating material. Phagocytic activity increased with increasing ionic strength of the coating material from PEG–SPIOs (lowest uptake) to starch–, CDX–, and PAA–SPIOs. The results for macrophage uptake were reciprocal to the blood half-life (Figures 5 and 6; note that for better visualization in Figure 6, the SPIOs with different coatings are arranged in reverse order compared to Figure 5). Higher iron uptake by macrophages is correlated with shorter blood kinetics.

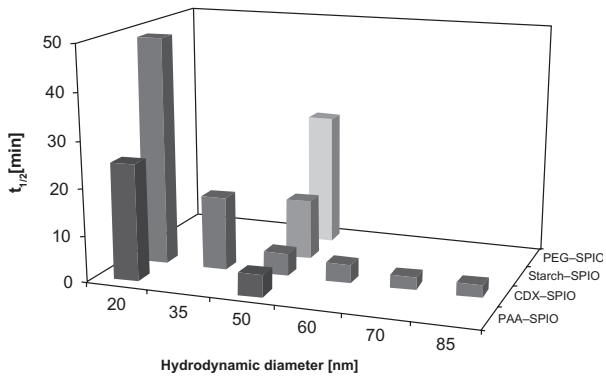

Figure 5 The blood half-life is dependent on the particle size and coating material.
Notes: SPIOs were injected at a dose of 100 μmol kg^{-1}, and blood samples were taken pre and post injection up to 360 minutes. The iron concentration was determined in plasma by ICP–OES and used to calculate the half-life. Values represent mean of $n \geq 3$ rats.
Abbreviations: CDX, carboxydextran; ICP-OES, inductively coupled plasma optical emission spectroscopy; PAA, polyacrylic acid; PEG, polyethylene glycol; SPIO, superparamagnetic iron oxide nanoparticle.

Discussion

For MRI that uses SPIOs as a contrast agent, two characteristics are essential: the magnetic behavior determines the signal achievable strength and the pharmacokinetic behavior determines the time point or frame for optimal image acquisition. Both characteristics are dependent on several SPIO properties, including the size and the coating material, in addition to inherently linked parameters, such as crystallinity, crystallographic phase, and impurities.

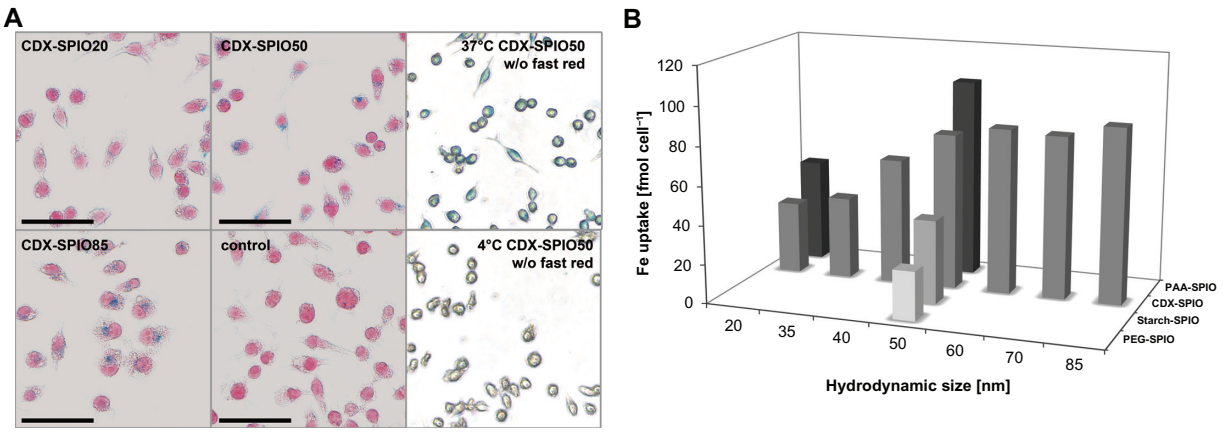

Figure 6 Size- and coating-dependent uptake by macrophages. P388D1 cells were incubated with 300 μmol L^{-1} SPIO solution for 4 hours at 37°C. (**A**) Prussian blue stain of phagocytized SPIOs. Representative images of cells incubated with CDX–SPIO20, CDX–SPIO50, and CDX–SPIO85 are shown exemplarily. Cells incubated without SPIOs served as control as well as cells incubated with CDX–SPIO50 at 4°C. (**B**) SPIO uptake was obtained by iron determination in the washed cells.
Note: Values represent means of at least four experiments.
Abbreviations: CDX, carboxydextran; PAA, polyacrylic acid; PEG, polyethylene glycol; SPIO, superparamagnetic iron oxide nanoparticle.

In contrast to previous studies, in our study the influence of one particular parameter on blood half-life and magnetic properties was systematically examined independently of other parameters. Two groups of SPIOs were studied: (1) SPIOs coated with polymers with different ionic strengths (PEG, starch, CDX, and PAA) but an identical hydrodynamic size (50 nm) and (2) SPIOs with different sizes (19–86 nm) but the same coating (CDX or PAA).

The magnetic properties of these SPIOs were analyzed by SQUID, and the influence of this property on proton relaxivity was measured by time-domain NMR. The SQUID data showed the superparamagnetic behavior of the synthesized nanoparticles. For the SQUID measurements the SPIOs were not fixed in solution but were dependent on Brownian motion, ie, free rotation of the magnetization in the liquid. Therefore no remnant magnetization at 300 K can be observed in solution. This effect is described as quasi-superparamagnetic behavior.[14] Therefore, all examined SPIOs were characterized by (quasi-) superparamagnetic behavior in solution. The saturation magnetizations were close to the values of magnetite and maghemite bulk material, which are 92 emu g^{-1} and 78 emu g^{-1}, respectively, at room temperature.[15] The r_2 relaxivity of the SPIOs increased linearly with increasing hydrodynamic particle size. A maximum was reached at 60 nm, and r_2 remained constant for larger SPIOs. The same behavior was described by Pöselt et al according to motional average regime (MAR) and static dephasing regime (SDR) theory.[16] In the first-regime MAR, r_2 increases with increasing size. At a certain particle size, r_2 no longer increases with increasing cluster size. This is the second regime SDR. In this regime, the particle size is so large that water molecules feel a constant magnetic field during their relaxation, resulting in a constant r_2 in this regime. In our case the second regime was observed for SPIOs larger than 60 nm. In Table 1, the r_2 values in different media are summarized for all SPIOs. The slightly higher r_2 values in plasma were attributed to the higher viscosity of plasma compared to water, as reported by Rohrer et al.[17]

The magnetic characteristics are comparable for the 50 nm SPIOs with different coatings (PAA, CDX, starch, and PEG). PAA–, PEG–, and starch–SPIOs have the same magnetic core. In a magnetic field the reaction of these cores is comparable, and the polymer layer did not significantly contribute to the formation and orientation of already existing magnetic domains and/or crystalline structure, as expected. Moreover, comparable r_2 values for SPIOs with different coating types were measured. The relaxivity was strongly affected by the size of the SPIOs, but the coating type had no substantial effect on this characteristic for the coating materials that were chosen for this study.

Pharmacokinetics is the second important characteristic of an SPIO contrast agent and is also relevant for other medical SPIO applications, such as hyperthermia and drug delivery. Moreover, pharmacokinetic data provide valuable information for the field of nanotoxicology. In this study we systematically showed that both the particle size and the coating material influenced blood kinetics independent of each other. As a blood-pool contrast agent, the SPIO blood kinetics are exclusively determined by SPIO distribution in the vessels and the elimination phase. Elimination is mainly mediated by clearance through uptake by the MPS. Larger

SPIOs cause higher iron uptake by macrophages. These results are in agreement with published reports. Larsen et al found that the uptake of PEG–SPIOs was eightfold higher when the SPIO size was increased from 20 nm to 40 nm.[18] Tabata and Ikada showed that macrophage uptake is increased with microsphere sizes up to 1.5 μm in diameter.[19] Our results show that SPIO uptake was not further increased if particle sizes larger than 60 nm were reached. The differences in uptake of SPIOs that only differed in size were directly mirrored in the in vivo situation. Macrophage uptake and blood kinetics are inversely correlated. For larger mean SPIO diameters, more iron was taken up by macrophages and the blood half-lives were shorter. This effect may have been enhanced by the slower diffusion rate of larger particles. Before being taken up by macrophages, SPIOs need to cross the fenestrated endothelial barrier in the sinusoids of the liver. Smaller SPIOs diffuse faster in and out than larger SPIOs. The time to be recognized and phagocytized by macrophages is short for small particles. Larger SPIO diffuse slower; if diffused through the endothelium, they have to remain long enough to be phagocytized. A systematic study with PEGylated gold nanoparticles is in agreement with our blood half-life results.[20] The blood half-life for those particles is dependent on size in a range of 25–86 nm. Interestingly, the blood half-life as determined by radiolabeling of the polymer on the gold nanoparticles is in the range of 0.4–50 hours, which is a long period of time for mice. For iron oxide particles only a few studies are available, but no systematic examination was found, Weissleder et al showed that 11-nm ultrasmall iron oxide particles fractionated from broadly size-distributed dextran-coated SPIO (AMI–25, volume median diameter of 72 nm) circulate much longer in rats (81 minutes) than the original preparation (6 minutes).[3] In contrast to our results, Chouly et al stated that below a threshold size of 50 nm, there is no detectable influence on biodistribution.[8] However, this study's conclusion was based on biodistribution results that were obtained for a single time point (20 minutes post injection). In the blood clearance plot shown for three of the particles, the differences are larger at earlier time points, underlining the importance of appropriate data sampling and kinetic studies, with time frames that are adjusted to the expected blood half-life. No blood half-lives were determined from the clearance plot.

Macrophage uptake and blood kinetics are also dependent on the coating material. The coatings used in this study are characterized by their different ionic characteristics. PAA is a polyanion, where each repeating unit exhibits a carboxylic acid function. CDX is a dextran containing terminal carboxylic groups. In starch, no ionic groups are present apart from a few that resulted from the mild oxidative conditions during the synthesis process. PEG is a fully nonionic coating material that exclusively exhibits polar heteroatoms.

Identically sized SPIOs were taken up more efficiently by macrophages when the ionic character was higher. Scavenger receptors on macrophages can recognize such polyanionic structures and mediate the phagocytosis of those materials.[21] Additionally a different opsonization pattern of the coating material may influence phagocytosis. That cellular uptake is influenced by the particle surface was shown in a comprehensive cell uptake screening of aminated cross-linked dextran SPIOs modified with 146 different small molecules.[22] Although some promising hits were found, no systematic conclusion was described. It is known that hydrophilic uncharged poly(ethylene glycol) has a stealth effect on macrophage recognition. Folic acid-coated particles were taken up more efficiently than PEGylated particles.[23] The PEGylation of starch–SPIOs led to a reduced uptake by macrophages, although the hydrodynamic diameter was larger.[9] This is one of the few studies that examined macrophage uptake as well as blood kinetics. The plasma half-life of the PEGylated starch–SPIOs was ten times longer than unmodified starch–SPIOs; however, size was also changed. The same effect was observed for dextran and CDX–SPIOs.[10] Similarly, dextran-coated SPIOs (AMI–227, 20–50 nm) exhibited a prolonged blood half-life of 2–3 hours in rats compared to CDX–SPIOs (SHU–555 C, 20 nm), although the mean hydrodynamic diameter of AMI–227 was larger. Besides the discussed reasons for alterations in macrophage uptake, it cannot be excluded that the different coating materials exhibit slight nonspecific interactions with the endothelium or components of the blood, which may additionally influence blood half-life.

Although SPIO uptake by macrophages was size and coat dependent, they were cleared via the MPS, but within different time ranges. Consequently, a high SPIO signal was found in the liver for all SPIO types (data not shown). After macrophage uptake, iron of the SPIOs is recycled into the endogenous iron metabolism. By 24 h post injection, substantial amounts of the injected dose could be found in the blood cell fraction for small and large PAA–SPIO (data not shown), indicating assembly of SPIO iron in the hemoglobin of erythrocytes.

Conclusion

In our study we systematically demonstrated the common opinion that SPIO size and coating influence blood kinetics

independently. By changing one specific parameter without modifying other parameters, we found that the magnetic properties and blood kinetics were strongly dependent on particle size. In contrast, the coating material has a less pronounced impact on magnetic properties and r_2 relaxivity; but its influence on blood kinetics is strong. Thus, for an on-demand design of an ideal T_2 contrast agent with a desired circulation time and strong contrast, it is more efficient to change the coating without changing the particle's magnetic properties than to modify the particle size. Smaller SPIOs are interesting as T_1 contrast agents with low ratios of r_2/r_1. These data provide a guideline information for the selection of a contrast agent for a specific application.

Acknowledgments/disclosure

The authors report no conflicts of interest in this work. The authors thank Claudia Heyer, Martin Kohs, Stefanie Runge, Erik Trinks, and Robert Ivkic from Bayer Pharma AG for their excellent technical assistance and Prof Dr Ulrich Pison from TOPASS GmbH for his support for part of the in vivo experiments.

References

1. Chen B, Wu W, Wang X. Magnetic iron oxide nanoparticles for tumor-targeted therapy. *Curr Cancer Drug Targets.* 2011;11(2):184–189.
2. Laurent S, Dutz S, Hafeli UO, Mahmoudi M. Magnetic fluid hyperthermia: focus on superparamagnetic iron oxide nanoparticles. *Adv Colloid Interface Sci.* 2011;166(1–2):8–23.
3. Weissleder R, Elizondo G, Wittenberg J, Rabito CA, Bengele HH, Josephson L. Ultrasmall superparamagnetic iron oxide: characterization of a new class of contrast agents for MR imaging. *Radiology.* 1990;175(2):489–493.
4. Thorek DL, Chen AK, Czupryna J, Tsourkas A. Superparamagnetic iron oxide nanoparticle probes for molecular imaging. *Ann Biomed Eng.* 2006;34(1):23–38.
5. Almeida JP, Chen AL, Foster A, Drezek R. In vivo biodistribution of nanoparticles. *Nanomedicine (Lond).* 2011;6(5):815–835.
6. Simberg D, Park JH, Karmali PP, et al. Differential proteomics analysis of the surface heterogeneity of dextran iron oxide nanoparticles and the implications for their in vivo clearance. *Biomaterials.* 2009;30(23–24):3926–3933.
7. Geng Y, Dalhaimer P, Cai S, et al. Shape effects of filaments versus spherical particles in flow and drug delivery. *Nat Nanotechnol.* 2007;2(4):249–255.
8. Chouly C, Pouliquen D, Lucet I, Jeune JJ, Jallet P. Development of superparamagnetic nanoparticles for MRI: effect of particle size, charge and surface nature on biodistribution. *J Microencapsul.* 1996;13(3):245–255.
9. Cole AJ, David AE, Wang J, Galban CJ, Hill HL, Yang VC. Polyethylene glycol modified, cross-linked starch-coated iron oxide nanoparticles for enhanced magnetic tumor targeting. *Biomaterials.* 2011;32(8):2183–2193.
10. Simon GH, von Vopelius-Feldt J, Fu Y, et al. Ultrasmall supraparamagnetic iron oxide-enhanced magnetic resonance imaging of antigen-induced arthritis: a comparative study between SHU 555 C, ferumoxtran-10, and ferumoxytol. *Invest Radiol.* 2006;41(1):45–51.
11. Lohrke J, Briel A, Mäder K. Characterization of superparamagnetic iron oxide nanoparticles by asymmetrical flow-field-flow-fractionation. *Nanomedicine.* 2008;3(4):437–452.
12. Hasegawa M, Hokkoku S, Inventors; Meito Sangyo Kabushiki Kaisha (Nagoya, JP), assignee. Magnetic iron oxide-dextran complex and process for its production US patent 4101435. Jun 14, 1976.
13. Saywell L, Cunningham B. Determination of iron: colorimetric o-phenanthroline method. *Industrial and Engineering Chemistry Analytical Edition.* 1937;9(2):67–69.
14. Miguel OB, Gossuin Y, Morales MP, Gillis P, Muller RN, Veintemillas-Verdaguer S. Comparative analysis of the 1H NMR relaxation enhancement produced by iron oxide and core-shell iron-iron oxide nanoparticles. *Magn Reson Imaging.* 2007;25(10):1437–1441.
15. Cullity BD, Graham CD. *Introduction to magnetic materials*. Philadelphia, PA: Wiley-IEEE Press; 2009.
16. Poselt E, Kloust H, Tromsdorf U, et al. Relaxivity optimization of a PEGylated iron-oxide-based negative magnetic resonance contrast agent for T(2)-weighted spin-echo imaging. *ACS Nano*. 2012;6(2):1619–1624.
17. Rohrer M, Bauer H, Mintorovitch J, Requardt M, Weinmann HJ. Comparison of magnetic properties of MRI contrast media solutions at different magnetic field strengths. *Invest Radiol.* 2005;40(11):715–724.
18. Larsen EK, Nielsen T, Wittenborn T, et al. Size-dependent accumulation of PEGylated silane-coated magnetic iron oxide nanoparticles in murine tumors. *ACS Nano.* 2009;3(7):1947–1951.
19. Tabata Y, Ikada Y. Effect of the size and surface charge of polymer microspheres on their phagocytosis by macrophage. *Biomaterials.* 1988;9(4):356–362.
20. Perrault SD, Walkey C, Jennings T, Fischer HC, Chan WC. Mediating tumor targeting efficiency of nanoparticles through design. *Nano Lett.* 2009;9(5):1909–1915.
21. Platt N, Gordon S. Scavenger receptors: diverse activities and promiscuous binding of polyanionic ligands. *Chem Biol.* 1998;5(8):R193–R203.
22. Weissleder R, Kelly K, Sun EY, Shtatland T, Josephson L. Cell-specific targeting of nanoparticles by multivalent attachment of small molecules. *Nat Biotechnol.* 2005;23(11):1418–1423.
23. Zhang Y, Kohler N, Zhang M. Surface modification of superparamagnetic magnetite nanoparticles and their intracellular uptake. *Biomaterials.* 2002;23(7):1553–1561.